

## A cascaded laser acceleration scheme for the generation of spectrally controlled proton beams

This article has been downloaded from IOPscience. Please scroll down to see the full text article.

2010 New J. Phys. 12 103009

(<http://iopscience.iop.org/1367-2630/12/10/103009>)

View [the table of contents for this issue](#), or go to the [journal homepage](#) for more

### Download details:

IP Address: 18.51.1.228

The article was downloaded on 19/03/2012 at 13:54

Please note that [terms and conditions apply](#).

## A cascaded laser acceleration scheme for the generation of spectrally controlled proton beams

S M Pfoth<sup>1,6</sup>, O Jäkel<sup>1,2</sup>, J Polz<sup>1</sup>, S Steinke<sup>3</sup>,  
H-P Schlenvoigt<sup>1,7</sup>, J Heymann<sup>1,8</sup>, A P L Robinson<sup>4</sup>  
and M C Kaluza<sup>1,2,5</sup>

<sup>1</sup> Institut für Optik und Quantenelektronik, Friedrich-Schiller-Universität Jena, Max-Wien-Platz 1, 07743 Jena, Germany

<sup>2</sup> Helmholtz-Institut Jena, Helmholtzweg 4, 07743 Jena, Germany

<sup>3</sup> Max Born Institut, Max-Born-Straße 2a, 12489 Berlin, Germany

<sup>4</sup> Central Laser Facility, STFC, Rutherford-Appleton Laboratory, Harwell Science and Innovation Campus, Didcot, OX11 0QX, UK

E-mail: [malte.kaluza@uni-jena.de](mailto:malte.kaluza@uni-jena.de)

*New Journal of Physics* **12** (2010) 103009 (11pp)

Received 3 March 2010

Published 5 October 2010

Online at <http://www.njp.org/>

doi:10.1088/1367-2630/12/10/103009

**Abstract.** We present a novel, cascaded acceleration scheme for the generation of spectrally controlled ion beams using a laser-based accelerator in a ‘double-stage’ setup. An MeV proton beam produced during a relativistic laser–plasma interaction on a thin foil target is spectrally shaped by a secondary laser–plasma interaction on a separate foil, reliably creating well-separated quasi-monoenergetic features in the energy spectrum. The observed modulations are fully explained by a one-dimensional (1D) model supported by numerical simulations. These findings demonstrate that laser acceleration can, in principle, be applied in an additive manner.

<sup>5</sup> Author to whom any correspondence should be addressed.

<sup>6</sup> Current address: Massachusetts Institute of Technology, 77 Massachusetts Avenue, E40-379, Cambridge, MA 02139-4307, USA.

<sup>7</sup> Current address: Laboratoire LULI, École Polytechnique, 91128 Palaiseau CEDEX, France.

<sup>8</sup> Current address: Institute of Environmental Physics and Remote Sensing, Universität Bremen, FB1 PO Box 330440, 28334 Bremen, Germany.

**Contents**

<b>1. Introduction</b>	<b>2</b>
<b>2. Experimental setup</b>	<b>3</b>
<b>3. Results of cascaded laser ion acceleration</b>	<b>4</b>
3.1. Spectral control . . . . .	4
3.2. Feasibility of setup to generate narrow-band spectral peaks . . . . .	6
3.3. Energy gain scaling for staged acceleration . . . . .	7
3.4. Numerical simulations of the double-stage setup . . . . .	7
<b>4. Conclusion</b>	<b>8</b>
<b>Acknowledgments</b>	<b>9</b>
<b>References</b>	<b>10</b>

**1. Introduction**

The rapid development in ultra-intense laser technology has resulted in a new generation of particle accelerators, which access a parameter regime complementary to that of conventional accelerators. Relativistic plasmas [1, 2] generated during the interaction of multi-terawatt (TW) laser pulses with matter have been identified as a brilliant source of GeV electrons [3, 4], MeV ions [5] and versatile photon beams [6]–[8]. The produced ion beams possess a number of unique properties, including ultra-short pulse duration, excellent emittance values and ultra-high peak currents [9], while requiring but minute acceleration lengths of several tens of micrometers. An important proof of the potential has recently been demonstrated with the availability of monoenergetic electron [10]–[13] and ion beams [14]–[19]. Thus, laser acceleration has opened up the possibility of many exciting applications, such as compact radiation sources for structural analysis [6, 20] and oncological therapy [21], as pre-accelerators for conventional acceleration devices [22], for medical isotope production [23] or for fast ignition of inertial confinement fusion [24, 25].

Especially for laser ion acceleration, however, the reliable generation of beams exhibiting a non-thermal or preferably quasi-monoenergetic spectrum still poses a substantial experimental challenge. Previous examples by our group have shown that using specially prepared targets with spatially confined ion sources allows for the generation of such quasi-monoenergetic ion pulses [15]. Although it has been shown that the position of the spectral peak scales with laser energy [18], the necessary reproducibility for applications and the required ease of spectral tuning have not yet been achieved. It is possible that laser ion accelerators will eventually have to rely on active beam shaping devices. However, in order to sustain the advantages of compact laser accelerators, these beam shaping devices should best be realized by laser acceleration, too, and hence act on the intrinsic timescale of the laser acceleration process and warrant the necessary flexibility. As a step towards these requirements, Toncian *et al* [17] proposed a laser-driven micro lens as an active energy selection device.

Here, we present a novel and reliable technique to actively control the proton spectrum on the required spatial and temporal scales. We demonstrate that a double-stage laser acceleration scheme can be utilized to characteristically modulate the proton spectrum of a proton beam created on a primary foil through a subsequent laser–plasma interaction on a separate, secondary foil. The principle of the cascaded acceleration scheme is depicted in figure 1. An MeV proton

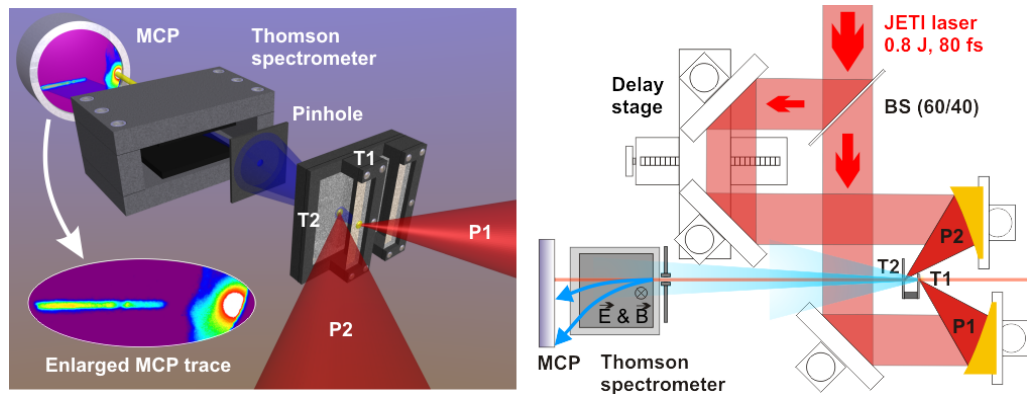


**Figure 1.** Experimental principle and setup. Interactions on two targets, T1 and T2, are triggered by two parts of the same laser pulse, P1 and P2. Protons accelerated from T1 and spectrally modulated on T2 are detected in a Thomson parabola equipped with a micro-channel plate (MCP) as the detector.

beam is generated by the laser pulse P1 at the primary target foil T1 via the mechanism of target normal sheath acceleration (TNSA). TNSA relies on the charge separation between a sheath of expelled electrons at the target rear side and the positively charged foil [26, 27]. Hydrogen contaminants present on the target surface are field ionized by the enormous electric fields in the  $\text{TV m}^{-1}$  range. Hence, protons are accelerated towards the secondary target T2, thereby undergoing dispersion. At T2, a second TNSA field is generated by the appropriately delayed second laser pulse P2, imposing a characteristic spectral modulation on the primary proton beam.

## 2. Experimental setup

Experiments were carried out with the Jena 10 TW titanium:sapphire laser system (JETI), which delivers pulses of 0.8 J energy and 80 fs pulse duration with an amplified spontaneous emission (ASE) contrast ratio of  $10^{-8}$  40 ps before the main pulse. The JETI pulses were split into two pulses (P1 and P2) by means of a 60/40 beam splitter (figure 1). Each pulse was focused with a  $45^\circ f/2$  off-axis parabolic mirror onto a  $2 \mu\text{m}$  thick titanium foil, which was mounted in series in a tandem frame at a fixed distance of 5.86 mm. The full-width at half-maximum (FWHM) focal spot areas were  $A_{P1} = 4.9 \mu\text{m}^2$  and  $A_{P2} = 6.6 \mu\text{m}^2$ , corresponding to intensities of  $I_{P1} = (1.7 \pm 0.1) \times 10^{19} \text{ W cm}^{-2}$  and  $I_{P2} = (0.7 \pm 0.1) \times 10^{19} \text{ W cm}^{-2}$ , respectively. The time-of-flight (TOF) of the protons for the propagation between T1 and T2 varied from  $\Delta\tau_{\text{delay}} = 600 \text{ ps}$  to  $267 \text{ ps}$  for proton energies of 0.5–2.0 MeV, which corresponds to an optical path difference of about  $\Delta s = 8\text{--}18 \text{ cm}$  between P2 and P1 realized by an optical delay line. The relative accuracy of the delay stage was given by a step width of  $2 \times 5 \mu\text{m}$  ( $\cong 33 \text{ fs}$ ), whereas the absolute delay stage position was determined with an accuracy of 1 mm ( $\cong 3 \text{ ps}$ ).

The ion beams were analyzed with a Thomson parabola spectrometer, using parallel magnetic (420 mT) and electric ( $2.6 \times 10^5 \text{ V m}^{-1}$ ) fields over an effective distance of 10 cm, and detected with a subsequent micro-channel plate (MCP), i.e. a spatially resolving secondary electron multiplier combined with a phosphor screen used in the Chevron setup. The MCP was absolutely calibrated both against CR39 nuclear track detector plastics and at the

TCC-CV28 cyclotron of the Physikalisch-Technische Bundesanstalt (German National Metrology Institute) in Braunschweig, Germany. Alternatively, CR39 plastics were used for detection. A pinhole in front of the spectrometer determined the solid angle of observation to  $1 \mu\text{sr}$ , corresponding to a spectral resolution of  $\sim 75 \text{ keV}$  at  $1 \text{ MeV}$ . Together with the source region of ion acceleration at the rear side of T1, the pinhole also defined the propagation axis of the protons detected in the spectrometer. The first target T1 had to be aligned perpendicular to this axis and the focus of P2 had to be centered to it in order to enable double-stage acceleration in an effectively one-dimensional (1D) geometry. This overlap was achieved by means of a robust alignment procedure with an accuracy of  $\sim 15 \mu\text{m}$ . In comparison, the TNSA proton source size on the foil—though varying with proton energy—is typically several hundred micrometers in diameter [28, 29].

### 3. Results of cascaded laser ion acceleration

#### 3.1. Spectral control

The results of double-stage acceleration are shown in figure 2(a). A strong modulation is observed on top of a quasi-exponential spectrum. Towards higher energies, one first encounters a region of proton accumulation, followed by a region of proton depletion and again accumulation. We interpret this modulation as follows: upon reaching T2, the duration of the proton pulse from T1 has increased to several hundred picoseconds and is hence much longer than the rapid TNSA field dynamics triggered by P2 at T2 [30, 31]. Therefore, only a fraction of the proton pulse is affected, which limits the influence to a narrow spectral region. In this transient field, however, those protons already behind T2 are further accelerated in the forward direction, while their slower successors are decelerated by the Coulomb wall at the target front. This re-acceleration and deceleration of protons corresponds to regions of proton accumulation in the spectrum, located on both sides of a central region of depletion as seen in figure 2(a).

Note that the total recorded spectra (figure 2(a), gray squares) originally contain proton contributions from both foils, as P2 also generates a separate but unmodulated proton beam with a quasi-thermal spectrum (i.e. an exponential with a characteristic quasi-temperature  $T_{\text{ion}}$ ) at T2. Explicit information about the primary proton beam (generated at T1 and modulated by the fields at T2) was obtained by subtracting an average background spectrum, recorded for sole irradiation of T2 with P2, from the compound spectra (resulting in the black squares in figure 2(a)). This assumes that the protons are only accelerated or decelerated but maintain their original direction, which is a viable first-order approximation for the (1D) geometry ensured by our alignment accuracy. All background spectra showed a Boltzmann-like energy distribution with an average temperature of  $k_{\text{B}}T_{\text{avg}} = 0.62 \pm 0.01 \text{ MeV}$ . The black squares spectrum in figure 2(a) therefore only represents those protons produced at T1, inserted externally into the second TNSA field and affected by it. For comparison, we show a proton spectrum that was obtained from the sole irradiation of T1 with P1 (as shown by the black line in figure 2(a)). Although slight changes in the total proton number can be observed (most likely due to shot-to-shot variations of the laser) when comparing the black line and black squares in figure 2(a), the strong modulation is only present in the case that both laser pulses irradiate the respective target foils.

All spectra recorded from the simultaneous irradiation of both foils exhibit the same characteristic modulation: the depth of the modulation is typically of the order of the total proton

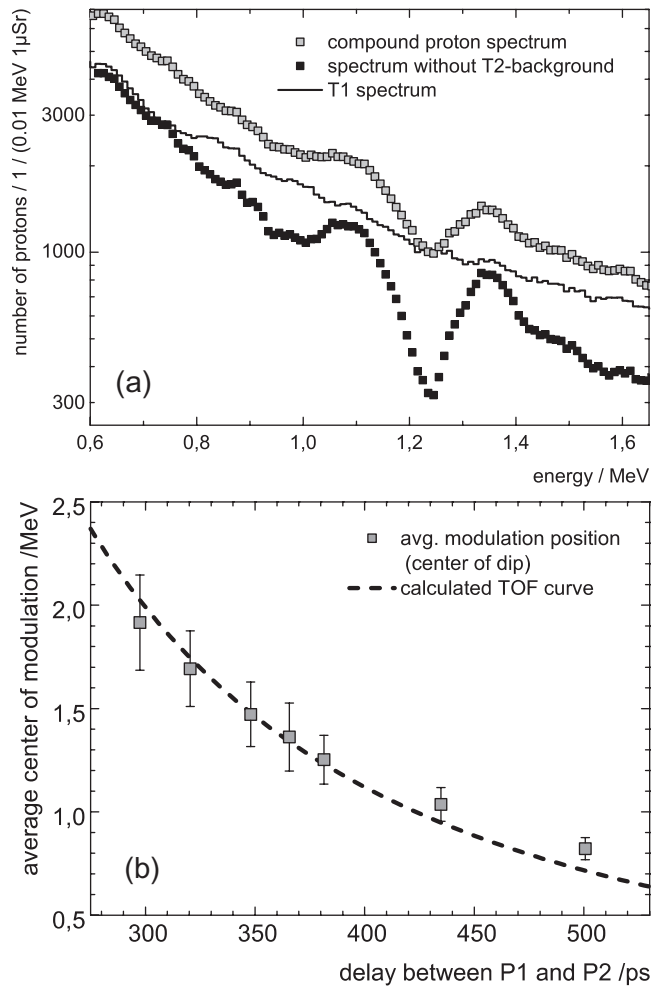


**Figure 2.** (a) Modulated proton spectra before (gray squares) and after (black squares) background subtraction. For comparison, we also show a proton spectrum as generated by P1 on T1 alone (black line). (b) Correlation between energy of the spectral depletion and delay between P1 and P2. The error bars indicate the standard deviation of the center position of the characteristic modulation for all shots recorded at a given delay stage setting.

signal strength, decreasing to almost zero in the depletion center, and piling up by a factor of  $\approx 1.5$  in the adjacent peaks. The center of the modulation therefore depends on the delay between pulses P1 and P2. In figure 2(a), the depletion center is located at  $E_{\text{center}} = 1.25 \pm 0.05$  MeV, which corresponds to a proton TOF of  $379 \pm 1$  ps for protons propagating from T1 to T2. This is in excellent agreement with the delay stage setting of  $\tau_{\text{delay}} = 378 \pm 3$  ps for this shot. Figure 2(b) shows how the position of the modulation varies with the delay time of P2, matching the theoretical TOF curve (dashed black line) excellently. The error bars indicate the standard deviation of the center position of the characteristic modulation for all shots recorded at a given delay stage TOF setting. This gives conclusive evidence that the observed spectral modulations and re-acceleration of protons can be attributed to the second TNSA field, and underline the reliability of the cascaded acceleration scheme.

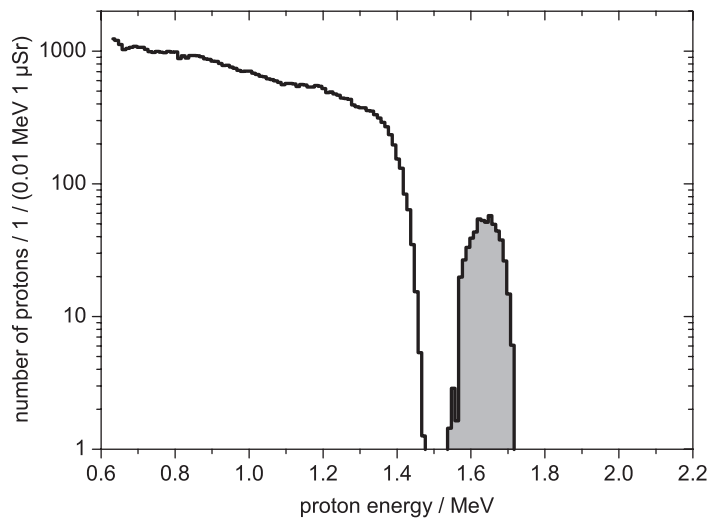


**Figure 3.** Acceleration of protons beyond the cutoff energy.

Note that the described use of the two consecutive interaction targets for laser-driven ion acceleration proved to be extremely robust. All spectra recorded from double-stage acceleration exhibited the same characteristic modulation, whereas the position of the modulation, defined by the dip center, fluctuated within less than  $\pm 200$  keV for high energies, and much less for lower energies, as displayed in figure 2(b). The number of re-accelerated protons contributing to the modulation at that energy thus typically varied by less than a factor of 2. Heavier ion traces were observed only from the P2–T2 interaction. Ions originating from the P1–T1 interaction, traveling at lower velocities than the protons, are stopped within T2 and have consequently not been observed.

### 3.2. Feasibility of setup to generate narrow-band spectral peaks

Given the above-mentioned flexibility of the re-acceleration impact over the full spectral width, the important question arises as to whether the double-stage setup can be used to accelerate the high-energy portion of the first proton beam beyond its original cutoff energy in order to produce a single, free-standing, quasi-monoenergetic peak. The experiments show that this is indeed possible: figure 3 presents the result of a shot where the delay stage setting was chosen to synchronize the incidence of P2 on T2 with the arrival of the fastest protons from the P1-generated beam. It can be seen that a distinct and well-separated proton peak was formed at an energy of 1.65 MeV with an FWHM bandwidth of 150 keV ( $\Delta E/E = 9\%$ ), approximately 200 keV higher in energy than the regular energy cutoff at 1.45 MeV of protons coming from T1 alone. Note that for the result shown in figure 3 the reduced cutoff energy of 1.45 MeV for P1 on T1 alone was obtained by slightly defocusing P1 impinging on T1 and hence reducing the corresponding intensity. Taking into account the opening angle of the beam of approximately  $10^\circ$  [9, 32], the solid angle of observation of the setup and the energy binning, the peak is found to contain about  $10^5$  protons re-accelerated by the T2 interaction. Well-separated quasi-monoenergetic peaks of this sort have been discussed as highly auspicious for a variety of potential applications before (cf [14, 15, 18] for more details).

The total proton number that is subjected to re-acceleration can be estimated by taking into account the relation between the total solid angle of T1 acceleration and the corresponding

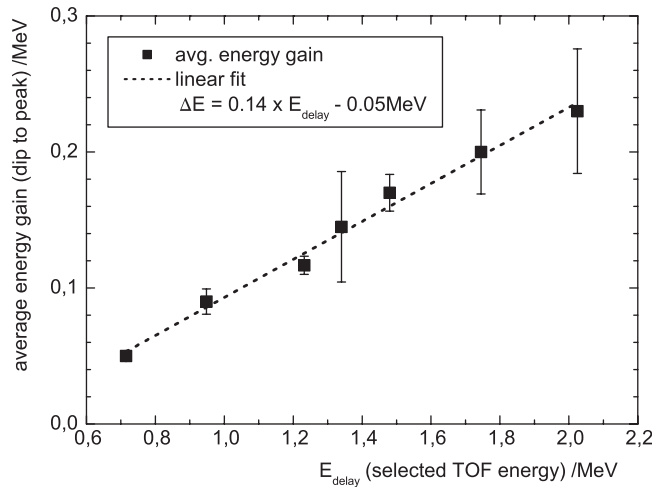


**Figure 4.** Scaling of the energy gain from double-stage acceleration as a function of the original (TOF) proton energy.

section due to the solid angle of the T2 interaction region. Reasonable assumptions are an opening angle of the proton beam of approximately  $10^\circ$  [9, 32] and a field extent of  $100 \mu\text{m}$  [29]. This results in the following solid angles: the initial acceleration cone occupies  $\approx 100$  msr, of which only 0.23 msr is affected at T2. Note that, in comparison, the solid angle of acceptance of the ion spectrometer is 0.001 msr only. For the peak of re-accelerated protons in figure 2(a), this gives  $10^4$  protons detected in the Thomson spectrometer, corresponding to a total number of  $2 \times 10^6$  protons that have been affected by the T2 interaction. Consequently, the peak in figure 3 corresponds to  $10^5$  protons re-accelerated by the T2 interaction.

### 3.3. Energy gain scaling for staged acceleration

A measure for the average energy gain due to the second acceleration can be derived from the energy difference between the depletion center and the center of the subsequent peak at higher energies. For all spectra, the energy gain follows approximately a linear function  $\Delta E = 0.14 \times E_{\text{delay}} - 0.05 \text{ MeV}$  with respect to the selected delay stage (TOF) energy (figure 4). At the same time, the relative energy gain  $\Delta E / E_{\text{delay}}$  gradually increases from 7.0% to 11.4%, whereas the slope  $0.14 \equiv 14\%$  of the linear function represents an asymptotic limit for the relative energy gain. Clearly, the energy gain achieved with the current two-stage setup does not yet compete with the maximum proton energies obtained with higher laser powers [18]. However, the observed transfer of protons from one part of the spectrum to regions of higher energy demonstrates that the particle energy can be enhanced successively by using multi-stage schemes.

### 3.4. Numerical simulations of the double-stage setup

To further substantiate our interpretation, we investigated the effect of a second laser–plasma interaction on the proton spectrum by means of numerical simulations. In the simulation, the T1-generated beam was followed through the P2–T2 interaction using a 1D3P electromagnetic Particle-In-Cell (PIC) code [33] that applies standard explicit PIC methods [34], and a



particle-tracking routine. Since the largest and the smallest relevant length-scales (i.e. the foil separation and the cold Debye length) are so disparate, a number of simplifying assumptions had to be made. Firstly, due to the velocity dispersion and transverse spatial spreading, the protons from T1 will be so rarefied by the time they reach T2 that they can be treated as test particles, not affecting the P2-generated fields. Secondly, it is assumed that the minimal description model required is 1D, and only the component of the electric field normal to the T2 foil is important. This assumption is justified given the alignment accuracy of our double-stage setup, which was better than  $15\ \mu\text{m}$  for the overlap between the two proton beam propagation axes. In contrast, the radial extent of the TNSA sheath is at least a factor of 10 larger for the present experimental conditions (cf e.g. [29, 33]). This alignment accuracy warrants that only the central, target-normal part of the second TNSA field is effectively used for re-acceleration, and transverse field components (i.e. parallel to the foil surface) can be neglected in the simulation.

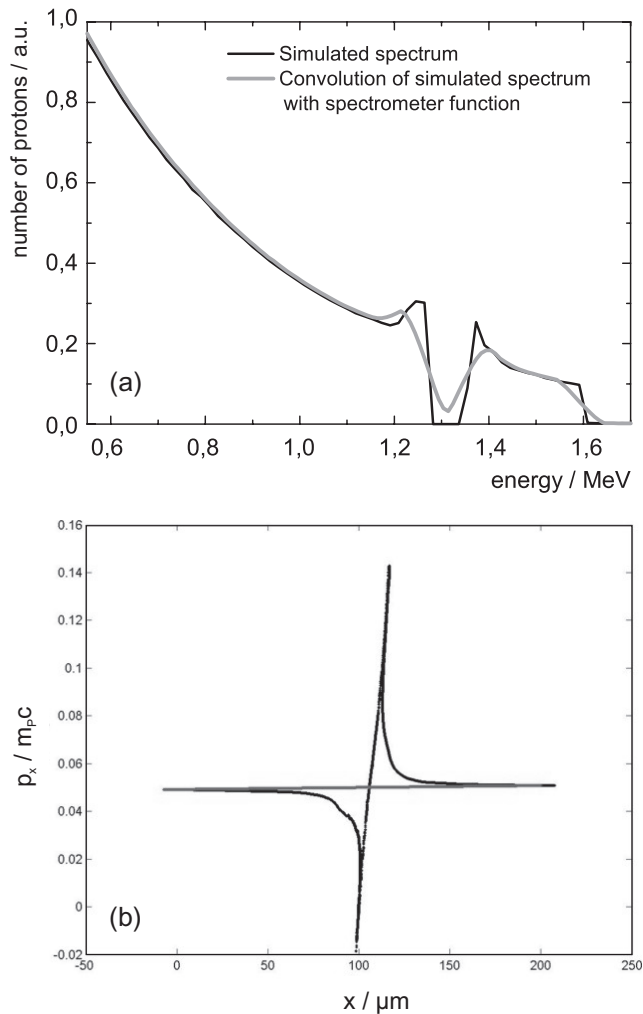
The electric fields of the P2 interaction are calculated by the 1D3P PIC code. The PIC results are then used to perform a subsequent ‘particle-tracking’ calculation for a sub-set of the P1 spectrum. This sub-set spanned those protons that had reached  $(5.86 \pm 0.08)$  mm after a delay time of 378 ps between the two pulses. The protons were represented by a set of macro-particles on a grid of the same dimensions as that used in the PIC simulation. The calculation was run up to 400 fs.

Figure 5(a) shows this spectrum (black line) with the expected modulation—the depletion region with the peaks at its boundaries—around  $1.30 \pm 0.05$  MeV. The simulated spectrum then had to be convolved with the spectrometer function to take into account the limited spectral resolution dominated by the aperture of 1 mm diameter used in the experiment. Including this convolution, one finds exactly the measured spectral shape (gray line). The positions of the features then amount to  $E_{\text{depl}} \approx 1.30 \pm 0.05$  MeV with  $E_{\text{dec}} \approx 1.20 \pm 0.05$  MeV and  $E_{\text{acc}} \approx 1.40 \pm 0.05$  MeV for the convolved spectrum, which is in excellent agreement with the measured spectrum, and its relative energy gain of 11.5% matches the results presented above.

The proton phase space is shown in figure 5(b) without (gray line) and with the second interaction (black line), with target T2 located at  $x = 100\ \mu\text{m}$ . Protons that are very close to T2 at the beginning of the second interaction are accelerated (or decelerated) the most, leading to a distinct loss of protons around a central energy. Protons that are farther away from P2 during the P2–T2 interaction experience a correspondingly weaker acceleration or deceleration. Consequently, the final proton distribution in phase space has two regions where the distribution has been ‘flattened’ at  $x \sim 50\ \mu\text{m}$  and  $x \sim 150\ \mu\text{m}$  compared to the positive slope of the unaffected distribution (gray trajectory). These regions correspond to the two peaks in the energy spectrum on either side of the central depletion energy. Moreover, the plot shows the acceleration of a few protons by a factor of 3 in momentum as well as deceleration up to a factor of 2.4, corresponding to a very encouraging energy gain of a factor of 9 for re-acceleration. However, these strongly accelerated protons were not observed during the experiment, most likely because their number was below the detection threshold of the spectrometer.

#### 4. Conclusion

In conclusion, we have demonstrated the first double-stage laser acceleration of protons, providing a very robust and flexible scheme for spectral shaping of laser-produced ion beams. Methodically inspired by staged schemes at conventional accelerators, the experiment also



**Figure 5.** (a) Spectrum achieved via numerical simulation of double-stage acceleration (black line) and convolved with spectrometer function (gray line). (b) Proton phase space without (gray line) and with (black line) second interaction.

showed for the first time that the TNSA mechanism can be applied in an additive manner. The energy band of the primary proton beam to be re-accelerated in the second field can be selected easily by altering the delay between the two laser pulses. The great robustness of the presented technique indicates the high potential to expand our scheme to multiple acceleration stages, where the benefits will be even stronger. Recent numerical simulations for multi-stage acceleration of monoenergetic proton beams predict an energy gain of up to a factor of 2 for the use of six stages [30, 35].

### Acknowledgments

This work was supported by DFG (contract no. TR18), BMBF (contract no. 03ZIK052) and the European Union (Laserlab Europe). We appreciate fruitful discussions with H Schworer, G G Paulus, T Sokollik, M Schnürer, P V Nickles, W Sandner and K W D Ledingham and we

thank B Beleites, F Ronneberger and W Ziegler for their excellent support. APLR is grateful for the use of computing resources provided by Science and Technology Facilities Council's e-Science facility.

## References

- [1] Mourou G A, Tajima T and Bulanov S V 2006 Optics in the relativistic regime *Rev. Mod. Phys.* **78** 309–71
- [2] Umstadter D 2001 Review of physics and applications of relativistic plasmas driven by ultra-intense lasers *Phys. Plasmas* **8** 1774–85
- [3] Leemans W P, Nagler B, Gonsalves A J, Toth C, Nakamura K, Geddes C G R, Esarey E, Schroeder C B and Hooker S M 2006 GeV electron beams from a centimetre-scale accelerator *Nature Phys.* **2** 696–9
- [4] Karsch S *et al* 2007 GeV-scale electron acceleration in a gas-filled capillary discharge waveguide *New J. Phys.* **9** 415
- [5] Snavely R A *et al* 2000 Intense high-energy proton beams from petawatt-laser irradiation of solids *Phys. Rev. Lett.* **85** 2945–8
- [6] Schlenvoigt H P *et al* 2008 A compact synchrotron radiation source driven by a laser-plasma wakefield accelerator *Nature Phys.* **4** 130–3
- [7] Schwoerer H, Liesfeld B, Schlenvoigt H P, Amthor K U and Sauerbrey R 2006 Thomson-backscattered x rays from laser-accelerated electrons *Phys. Rev. Lett.* **96** 014802
- [8] Schwoerer H, Gibbon P, Düsterer S, Behrens R, Ziener C, Reich C and Sauerbrey R 2001 MeV x-rays and photoneutrons from femtosecond laser-produced plasmas *Phys. Rev. Lett.* **86** 2317–20
- [9] Cowan T E *et al* 2004 Ultralow emittance, multi-MeV proton beams from a laser virtual-cathode plasma accelerator *Phys. Rev. Lett.* **92** 204801
- [10] Faure J, Glinec Y, Pukhov A, Kiselev S, Gordienko S, Lefebvre E, Rousseau J P, Burgy F and Malka V 2004 A laser-plasma accelerator producing monoenergetic electron beams *Nature* **431** 541–4
- [11] Geddes C G R, Toth C, van Tilborg J, Esarey E, Schroeder C B, Bruhwiler D, Nieter C, Cary J and Leemans W P 2004 High-quality electron beams from a laser wakefield accelerator using plasma-channel guiding *Nature* **431** 538–41
- [12] Mangles S P D *et al* 2004 Monoenergetic beams of relativistic electrons from intense laser-plasma interactions *Nature* **431** 535–8
- [13] Hidding B *et al* 2006 Generation of quasimonoenergetic electron bunches with 80-fs laser pulses *Phys. Rev. Lett.* **96** 105004
- [14] Hegelich B M, Albright B J, Cobble J, Flipppo K, Letzring S, Paffett M, Ruhl H, Schreiber J, Schulze R K and Fernandez J C 2006 Laser acceleration of quasi-monoenergetic MeV ion beams *Nature* **439** 441–4
- [15] Schwoerer H, Pfoth S, Jäckel O, Amthor K U, Liesfeld B, Ziegler W, Sauerbrey R, Ledingham K W D and Esirkepov T 2006 Laser-plasma acceleration of quasi-monoenergetic protons from microstructured targets *Nature* **439** 445–8
- [16] Ter-Avetisyan S, Schnürer M, Nickles P V, Kalashnikov M, Risse E, Sokollik T, Sandner W, Andreev A and Tikhonchuk T 2006 Quasimonoenergetic deuteron bursts produced by ultraintense laser pulses *Phys. Rev. Lett.* **96** 145006
- [17] Toncian T *et al* 2006 Ultrafast laser-driven microlens to focus and energy-select mega-electron volt protons *Science* **312** 410–3
- [18] Pfoth S M *et al* 2008 Spectral shaping of laser generated proton beams *New J. Phys.* **10** 33034
- [19] Henig A *et al* 2009 Radiation-pressure acceleration of ion beams driven by circularly polarized laser pulses *Phys. Rev. Lett.* **103** 245003
- [20] Fuchs M *et al* 2009 Laser-driven soft-x-ray undulator source *Nature Phys.* **5** 826–9
- [21] Bulanov S V, Esirkepov T Z, Khoroshkov V S, Kunetsov A V and Pegoraro F 2002 Oncological hadron-therapy with laser ion accelerators *Phys. Lett. A* **299** 240–7

- [22] Krushelnick K *et al* 2000 Ultrahigh-intensity laser-produced plasmas as a compact heavy ion injection source *IEEE Trans. Plasma Sci.* **28** 1184–9
- [23] Ledingham K W D, McKenna P and Singhal R P 2003 Applications for nuclear phenomena generated by ultra-intense lasers *Science* **300** 1107–11
- [24] Hora H *et al* 2007 Fast ignition by laser driven particle beams of very high intensity *Phys. Plasmas* **14** 072701
- [25] Roth M *et al* 2001 Fast ignition by intense laser-accelerated proton beams *Phys. Rev. Lett.* **86** 436–9
- [26] Hatchett S P *et al* 2000 Electron, photon, and ion beams from the relativistic interaction of petawatt laser pulses with solid targets *Phys. Plasmas* **7** 2076–82
- [27] Wilks S C, Langdon A B, Cowan T E, Roth M, Singh M, Hatchett S, Key M H, Pennington D, MacKinnon A and Snavely R A 2001 Energetic proton generation in ultra-intense laser-solid interactions *Phys. Plasmas* **8** 542–9
- [28] Roth M *et al* 2002 The generation of high-quality, intense ion beams by ultra-intense lasers *Plasma Phys. Control. Fusion* **44** (Suppl. 12B) B99–B108
- [29] Schreiber J *et al* 2004 Source-size measurements and charge distributions of ions accelerated from thin foils irradiated by high-intensity laser pulses *Appl. Phys. B* **79** 1041–5
- [30] Velchev I, Fourkal E and Ma C M 2007 Laser-induced coulomb mirror effect: applications for proton acceleration *Phys. Plasmas* **14** 033106
- [31] Fuchs J *et al* 2006 Laser-driven proton scaling laws and new paths towards energy increase *Nature Phys.* **2** 48–54
- [32] Kaluza M, Schreiber J, Santala M I K, Tsakiris G D, Eidmann K, Meyer-ter Vehn J and Witte K J 2004 Influence of the laser prepulse on proton acceleration in thin-foil experiments *Phys. Rev. Lett.* **93** 045003
- [33] Robinson A P L, Neely D, McKenna P and Evans R G 2007 Spectral control in proton acceleration with multiple laser pulses *Plasma Phys. Control. Fusion* **49** 373–84
- [34] Birdsall C K and Langdon A B 1991 *Plasma Physics via Computer Simulation* (New York: Hilger)
- [35] Fourkal E, Velchev I and Ma C M 2009 Laser-to-proton energy transfer efficiency in laser-plasma interactions *J. Plasma Phys.* **75** 235–50